Columnar mesophases of hexabenzocoronene derivatives. I. Phase transitions

Valentina Marcon,[1,a)] Thorsten Vehoff,[1] James Kirkpatrick,[1,2] Cheol Jeong,[3] Do Y. Yoon,[3] Kurt Kremer,[1] and Denis Andrienko[1,b)]
[1]*Max-Planck-Institut für Polymerforschung, Ackermannweg 10, 55128 Mainz, Germany*
[2]*Department of Physics, Imperial College London, Prince Consort Road, London SW7 2BW, United Kingdom*
[3]*Department of Chemistry, Seoul National University, Seoul 151-747, Republic of Korea*

(Received 15 April 2008; accepted 21 July 2008; published online 4 September 2008)

Using atomistic molecular dynamic simulations we study the transitions between solid herringbone and liquid crystalline hexagonal mesophases of discotic liquid crystals formed by hexabenzocoronene derivatives. Combining a united atom representation for the side chains with the fully atomistic description of the core, we study the effect of side chain substitution on the transition temperatures as well as molecular ordering in the mesophases. Our study rationalizes the differences in charge carrier mobilities in the herringbone and hexagonal mesophases, which is predominantly due to the better rotational register of the neighboring molecules. © *2008 American Institute of Physics*. [DOI: 10.1063/1.2969763]

I. INTRODUCTION

Organic π-conjugated materials are potential candidates for a number of emerging electronic devices, such as field effect transistors, light emitting diodes, and solar cells.[1,2] To arrive at molecular electronics based on these systems, a detailed understanding of the underlying physical properties of the corresponding materials is needed. In particular, values of charge carrier mobilities are crucial for their efficiency.[3] The latter is extremely sensitive to the material morphology, i.e., local ordering of molecules, which depends on the ability to self-assemble, the presence of structural defects, and of course on the type of the mesophase. While the quality of the molecular arrangement is mainly determined by choosing the right processing, the type of the mesophase and local ordering depend on the underlying chemistry of compounds.

Among π-conjugated materials discotic thermotropic liquid crystals are unique in the sense that they combine the properties of fluidity of liquids (easy to process, self-healing abilities) with the orientational order of crystals (anisotropic conducting and optical properties). The orientational order arises from the anisotropy of molecules: flat aromatic core with aliphatic chains attached at the edges. By tuning the shape and the size of the conjugated core, as well as the type of the attached side chains, compounds with different ability to self-organize and conduct charge carriers can be obtained. Synthetic design allows one to optimize the charge transport and to control the morphology on meso- and microscales.

It would, of course, be helpful to get an insight into the mesophase properties prior to the actual synthesis. In our previous work[4–6] we have shown that one can accurately describe the local arrangement of the molecules in small well-aligned domains using molecular dynamics (MD) and atomistic level of description.[7,8] This approach allowed one to study the effect of side chain substitution on the local packing of hexabenzocoronene derivatives. Based on the obtained morphologies, charge mobilities of columnar mesophases were calculated by computing the charge hopping rates within the Marcus–Hush formalism and by solving charge carrier dynamics with kinetic Monte Carlo; these mobilities were in excellent agreement with the values from pulse radiolysis time resolved microwave conductivity (PR-TRMC) (Refs. 9 and 10) experiments. These results, however, were obtained for the systems at two temperatures by fixing the (experimentally provided) symmetry of the mesophase. No attempts were made to observe the transitions between the different mesophases or to characterize the effect of temperature increase in the molecular ordering and charge mobilities in a single mesophase.

Differential scanning calorimetry (DSC) experiments, however, predict that several phase transitions can occur in discotic liquid crystals. Depending on temperature and on the nature of side chains, a herringbone, hexagonal, or rectangular molecular arrangement can be found.[9,11–17] Apart from the lattice symmetry change upon heating, PR-TRMC measurements reveal that charge carrier mobility is very sensitive to the mesophase symmetry. For example, it is about two times higher in a herringbone than in a hexagonal mesophase.[9,10] To understand the physical reasons behind this behavior, a detailed knowledge of molecular arrangement as a function of temperature is needed.

Prediction of phase transitions, however, is well-known to be problematic in computer simulation. First, one is bound to an atomistic level of description since the transition temperatures are sensitive to the chemical structure. On the other hand, the accuracy of interaction potentials, sample size and, even more important, equilibration times are limited. This

[a)]Electronic mail: marcon@mpip-mainz.mpg.de.
[b)]Electronic mail: denis.andrienko@mpip-mainz.mpg.de.

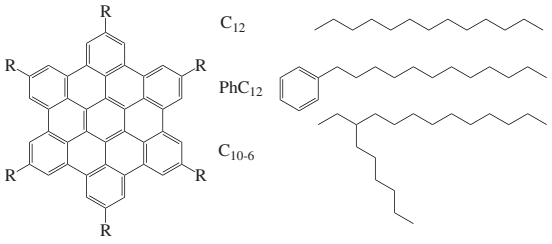

FIG. 1. Studied derivatives of hexabenzocoronene.

explains why in most cases, with some rare exceptions,[18–20] the full temperature dependence and mesophase transitions of liquid crystals have not been addressed.

This work is the first attempt to elucidate some of the phase transitions between three derivatives of hexabenzocoronenes: with linear alkane, branched, and dodecylphenyl-substituted side chains. At room temperature, these compounds are solids with either herringbone (alkane and branched side chains) or rectangular (dodecylphenyl-substituted side chains) molecular packing. At higher temperatures, they are liquid crystalline with the hexagonal ordering of columns. Performing thermal annealing, we observe the corresponding transitions and track changes in molecular ordering with the temperature change. This work is the onset for studies aiming at relating charge carrier mobilities to the arrangement of molecules in mesophases and to the role of the molecular ordering on temperature dependence of mobility.[21]

II. STUDIED SYSTEMS AND COMPUTATIONAL DETAILS

The molecular structures of the studied hexabenzocoronene derivatives are shown in Fig. 1. We considered three types of side chains: alkyl chains of length 12 (C_{12}); branched side chains, C_{10-6}; and dodecylphenyl-substituted PhC_{12} side chains. The choice of systems is based on our previous studies,[7] which show qualitatively different local mesophase orderings and, as a result, quantitatively different charge carrier mobilities.[4] In addition, these systems are well-characterized experimentally by various techniques: wide angle x-ray scattering (WAXS), solid state NMR, and DSC.[9,11–15] For charge transport, PR-TRMC data[9,10] and time of flight measurements of mobility[22,23] are also available.

A. Model potential

As in the previous study,[7] we use the united atom approach for the side chains and consider explicitly only the hydrogen atoms belonging to the aromatic rings of the central core.

Following Ref. 7 we define eight types of atom (see Fig. 2): aromatic carbons of the central ring (C_B), aromatic carbons bonded to the hydrogens (C_H), hydrogens (H), aliphatic carbons representing either a methylene group (C_2), terminal methyl group (C_3), or a junction (C_1), and aromatic carbons bonding either an alkyl chain (C_A) or two aromatic subsystems (C_P).

In this representation, the OPLS *all-atom* force field is used for the aromatic core and the OPLS *united* atom force field for the side chains. The side chains of interest have three distinct cases of attachment to the aromatic core: via a linear alkane, branched side chain, and phenyl ring. The standard OPLS force field does not have parameters describing the attachment of alkane chains to an aromatic core. In addition, two different representations, OPLS all atom and united atom, are used for the aromatic core and side chains. Hence, the parameters of three torsion potentials shall be obtained from quantum chemical calculations.

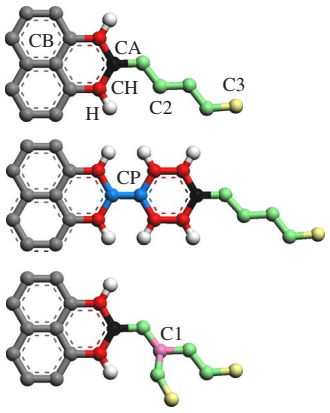

FIG. 2. (Color online) Atom types: aromatic carbons of the central ring (C_B), aromatic carbons bonded to the hydrogens (C_H), hydrogens (H), aliphatic carbons representing either a methylene group (C_2), terminal methyl group (C_3), or a junction (C_1), and aromatic carbons bonding either alkyl chain (C_A) or two aromatic subsystems (C_P).

To obtain the dihedral term for the attachment of either alkane or branched side chains to the aromatic core (for example, the dihedral $C_H-C_A-C_2-C_2$) we scan the corresponding angle, optimizing the molecular geometry for each dihedral angle using density functional theory (DFT) calculations (see Sec. II B for details). The potential energy of each structure is then evaluated using the known force-field parameters with the corresponding dihedral switched off. The difference between the DFT and force-field-based energies is then fitted, yielding the parametrization constants of the dihedral.

In some cases, apart from excluding the 1–4 interactions for the dihedral of interest, we have also removed the interaction of the aromatic hydrogens (connected to the aromatic carbons C_H) with the nearest united atoms in the chain (first two C_2 atoms). The corresponding nonbonded interactions are then incorporated directly into the dihedral potential.

1. Linear alkane side chains, C_{12}

Scanning the corresponding dihedral (with geometry optimization of the structures) showed that the torsion potential has a minimum at 90°, i.e., when the second bond is perpendicular to the plane of the core, which is in agreement with the previous studies.[24] This potential [see Fig. 3(a)] favors the reorientation of the side chains perpendicular to the core and therefore stabilizes the tilted arrangement of the molecules, like in the herringbone mesophase.

2. Phenyl rings

The potential energy surface for two phenyl rings rotating with respect to the linking bond has been studied in detail

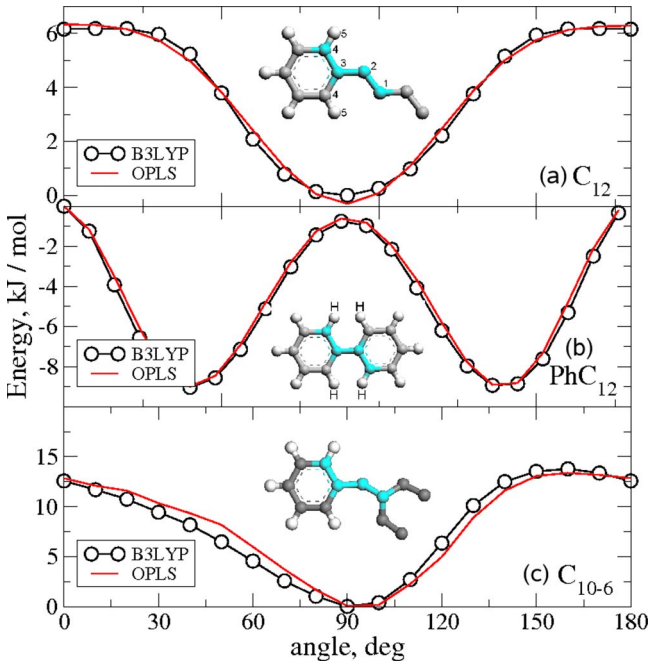

FIG. 3. (Color online) *Ab initio* and force-field based potential energy surfaces for (a) $C_H-C_A-C_2-C_2$ dihedral angle for the C_{12} side chains. All bond lengths were fixed during the force-field calculations, in addition to 1–4 interactions, the 1–5 interactions between the closest side chain carbon and the nearest core hydrogens were excluded. (b) $C_H-C_P-C_P-C_H$ dihedral angle. The nonbonded interactions between the hydrogens labeled with H were excluded. (c) Potential energy as a function of the $C_H-C_A-C_2-C_1$ dihedral angle.

in Ref. 25. In order to reproduce this potential, four interactions between the closest hydrogens were excluded [see Fig. 3(b)]. For this particular system, in line with the OPLS force-field convention, the 1–4 interactions were included, scaled down by a factor of 0.5 for both Coulomb and Lennard-Jones interactions.

3. Branched side chains, C_{10-6}

For the dove-tail side chain, 1–4 interactions were excluded along with interactions between the branching carbon and the two closest core hydrogens. All *ab initio* calculations were performed using a symmetric side chain configuration as a starting point. The side chain was chosen to be four united atoms long to increase the distance between the core and the bulky CH_3 moieties for the MD energy calculations.

The best fit was obtained using a cosine expansion up to the sixth order of magnitude

$$V = \sum_{n=0}^{6} V_n \cos^n \psi. \quad (1)$$

All parameters extracted from the fits to *ab initio* calculations are summarized in Table I. Note that in most force-field implementations (e.g., OPLS) the Ryckaert–Belleman function provides an expansion only up to the fifth order.

B. Computational details

Geometry optimization and determination of the parameters of bonded interactions were performed using the GAUSSIAN package.[26] We used the B3LYP functional with the 6-31G basis set for the branched side chain, 6-31G(d) for the C_{12} side chain, and 6-311G(d,p) for the phenyl rings. Several points were calculated using higher order methods [MP2, 6-31G(d,p) basis set]. No significant differences between the methods were found.

MD simulations were performed with the GROMACS program.[27] The electrostatic interaction was treated with the smooth particle-mesh Ewald (PME) method[28] (spacing for PME grid of 0.12 nm). The time step of 2 fs was used to integrate equations of motion using the velocity Verlet algorithm with 0.9 nm cutoff for short-range interactions. Bond lengths were constrained using LINCS algorithm.[29]

We simulated systems of up to 160 molecules, arranged in columns of ten molecules each. The initial configuration was either a herringbone one with the HBC cores tilted by 30° with respect to the plane normal to the columnar axis (C_{12}, C_{10-6}) or a rectangular arrangement of columns with the cores perpendicular to the columnar axis (PhC_{12}). The distance between the columns and the molecules in the columns has been slightly increased to avoid site superposition. After the energy minimization and a short equilibrating run (4 ns), production runs of 40 ns were performed at a constant pressure $P=0.1$ MPa, at different temperatures, using Parinello–Rahman barostat and Nóse–Hoover thermostat. The simulation box angles where fixed at 90°.

III. RESULTS

Typical MD simulation snapshots of the C_{12} system are shown in Fig. 4. The herringbone (300 K) mesophase has a tilt angle of about 30° and is well ordered. During the equilibration run, the tilt angle and the lattice parameters of the herringbone phase change, but the interlocking of the side chains remains practically the same. Contrary, the hexagonal mesophase has a disordered liquidlike arrangement of the side chains with a zero molecular tilt angle in columns.

To further characterize the mesophase ordering, several order parameters were calculated as a function of temperature.

TABLE I. Parameters of the torsional potential. C_i are given in kJ mol^{-1} for Ryckaert–Bellemans dihedrals and in kJ mol^{-1} rad^{-2} for improper dihedrals. Atom types correspond to those shown in Fig. 2.

Dihedral	V_1	V_2	V_3	V_4	V_5	V_6	Improper	K_d
$C_H-C_A-C_2-C_2$	−0.03	9.44	0.48	−5.16	−0.47	0.0	$C_H-C_H-C_A-C_2$	167.4
$C_H-C_P-C_P-C_H$	0.0	−37.02	0.0	23.09	0.0	0.0		
$C_H-C_A-C_2-C_1$	0.0	24.93	0.0	−31.55	0.0	15.07		

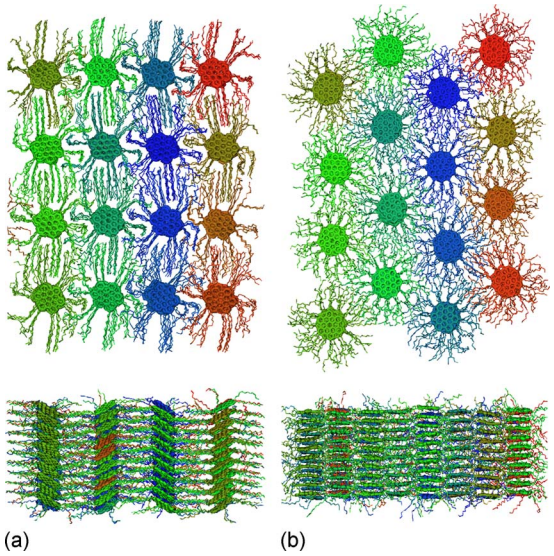

FIG. 4. (Color online) MD simulation snapshots of the derivative with C_{12} side chains: (a) herringbone (300 K) and (b) hexagonal (400 K) phases.

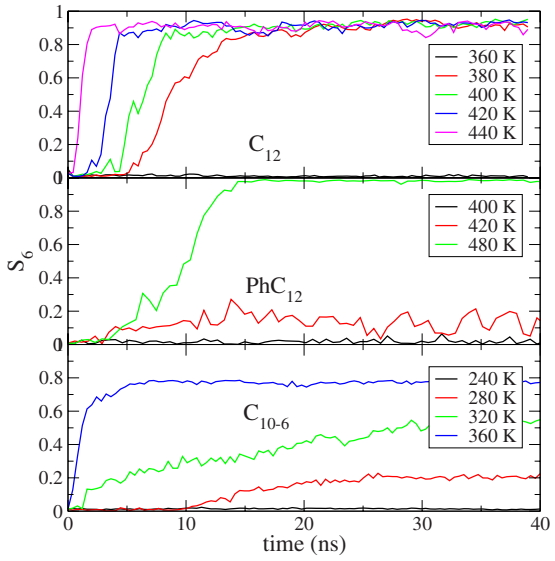

FIG. 5. (Color online) Time evolution of the S_6 order parameter for C_{12}, PhC_{12}, and C_{10-6} side chains for different heating temperatures. $S_6=1$ corresponds to a perfect hexagonal packing. All systems were prepared in a herringbone mesophase, equilibrated, and then run at different temperatures in the interval from 280 to 480 K.

A. Lattice order parameter

To elucidate the temperature-induced transition from herringbone to hexagonal packing, we have calculated two order parameters, S_4 and S_6,[30]

$$S_k = \left\langle \frac{\left|\sum_{i=0}^{n-1}\sum_{j=i+1}^{n} q_{ij}\exp(ik\phi_{ij})\right|}{\sum_{i=0}^{n}\sum_{j=i+1}^{n} q_{ij}} \right\rangle, \tag{2}$$

where $k=4,6$, ϕ_{ij} is the angle between the centers of mass of the molecules in the neighboring columns, $q_{ij}=1$ if r_{ij} belongs to the first peak of the radial distribution function, and zero otherwise. S_6 describes the degree of the order of the hexagonal arrangement of the columns. In the case of a perfect hexagonal order $S_6=1$, whereas $S_6=0$ indicates the complete lack of such order. Correspondingly, S_4 describes the degree of a rectangular ordering of columns on a lattice.

The time evolution of the instantaneous values of the S_6 lattice parameter is shown in Fig. 5. S_4 is not shown since it is complementary to S_6. One can see that all three systems have very different response to the temperature increase. In the case of C_{12} side chains, the herringbone phase is stable below 360 K. At 380 K, the lattice rearranges from herringbone to hexagonal after about 10 ns. If we further increase the quenching temperature, this transition occurs much earlier. We can, therefore, locate the transition between 360 and 380 K. DSC and charge transport measurements predict that this transition occurs at about 380 K.[12] However, one has to remember that, due to the final system size, simulations provide only the upper boundary for transition temperature, nonetheless the agreement is remarkable.

Contrary, the PhC_{12} system preserves rectangular columnar ordering (without molecular tilt) up to 420 K and then changes to a hexagonal one. This transition occurs much more slowly compared to the C_{12} systems and has also been observed experimentally[12,31] at about 400 K.

Finally, the C_{10-6} system has a herringbone orthorhombic packing up to 320 K. After 320 K, it changes to hexagonal packing of columns and develops domains of molecules with different tilts. The orientation of domains becomes more and more disordered and, if one keeps heating the system, the molecules in each column arrange in domains of 4–8 molecules, with different tilt angles, as it is shown in Fig. 6. The hexagonal arrangement of columns is, however, still preserved. Experimentally, a similar picture is observed for the transition of the monoclinic plastic crystalline phase into the columnar disordered phase. According to DSC, this transition occurs at 290 K; however, due to the finite size of the simulation box, the simulated transition temperatures are generally in the upper limits. One can imagine that the small packets of well ordered molecules would survive into the isotropic phase, confirming two-dimensional WAXS experiments,[10] which observed broad small-angle reflections, attributed to molecular aggregates of about 6 molecules.

B. Radial distribution functions

We have also calculated two spatial correlation functions, $g_z(r)$ and $g_{xy}(r)$. $g_z(r)$ provides information about the arrangement of the molecules in the planes parallel to the director $\boldsymbol{n}$, which, in our case, is the direction of the columns (along the z axis). In other words, $g_z(r)$ is the probability to find a molecule at a distance $\boldsymbol{n}\cdot\boldsymbol{r}$ from the reference molecule,

$$g_z(r) = \frac{2}{VN}\sum_{\text{columns}}\sum_{i=0}^{N_c}\sum_{j>i}^{N_c} f(\boldsymbol{r},\boldsymbol{n}\cdot\boldsymbol{r}_{ij}), \tag{3}$$

where N_c is the number of the molecules in a column, r_{ij} is the distance between the centers of mass of molecules i and j, N is the total number of molecules in the system, f is a binning function—i.e., $f=1$ if $\boldsymbol{n}\cdot\boldsymbol{r}_{ij}\in[r\pm\Delta/2]$, where Δ is the bin size (in our case the number of bins was 400), otherwise $f=0$—and $V=\Delta L_x L_y$ is the volume of the bin. Note that averaging is first performed in each column and then

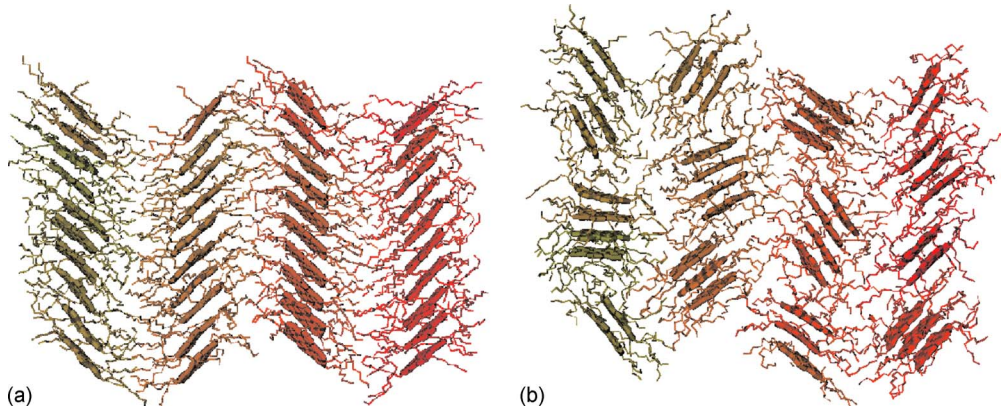

FIG. 6. (Color online) Snapshots of the C_{10-6} at 280 K (left) and at 480 K (right).

over the columns since the columns can diffuse with respect to each other. This distribution function can be related to the mobility of the charge carriers in the one-dimensional charge transport along the column.[4]

The second distribution function, g_{xy}, provides information on the arrangement of molecules in planes perpendicular to the director $\boldsymbol{n}$, in the xy plane

$$g_{xy}(r) = \frac{2}{V(r)N}\sum_{i=0}^{N}\sum_{j>i}^{N} f(\boldsymbol{r}, \boldsymbol{n}\times\boldsymbol{r}_{ij}), \tag{4}$$

where $V(r)$ is the volume of a cylindrical bin. It allows one to accurately determine the intercolumnar distance and the lattice parameters of the herringbone and hexagonal arrangement of columns.

g_z is shown in Fig. 7. For the C_{12} side chains, this distribution function has a clear peak at about 4.2 Å below 380 K, which corresponds to the tilted phase. Above 380 K, the peak shifts to 3.6 Å, which indicates that the molecules are perpendicular to the direction of columns. Note that g_z measures the projection of the distance between the molecular planes on the z axis changes; therefore, in both cases, the actual distance between the neighboring cores does not change and is always 3.6 Å. Also interesting is that g_z has a broader distribution (and correspondingly, lower amplitude of peaks) in the herringbone (low temperature) phase. This is due to the wider distribution of the molecular tilt angles in the herringbone phases compared to the hexagonal phase when they are flat.

In the case of PhC_{12}, the molecules are always perpendicular to the z axis for both the hexagonal and rectangular arrangements of the columns. Hence, there is no shift of the peaks. At low temperatures, each main peak is accompanied by a satellite one due to a small nonsystematic tilting of the molecules, which is due to out-plane fluctuations of the cores in the columns arranged on a rectangular lattice. At higher temperatures, the peaks sharpen and satellites disappear.

Finally, the system with the C_{10-6} side chains is the most disordered: the peaks are wide even in the herringbone mesophase, where the tilt angle is ~45° at 280 K. Here heating up does lead to the change in the lattice symmetry; however, the peaks do not become sharper, as in the rest of the systems. This is again understandable if one recalls that the domains of different molecular orientations are formed inside the columns, as it is shown in Fig. 6.

C. Nematic order parameter

To calculate the orientational order parameter we considered only the aromatic cores of the molecules. The plane of the core was specified by the six vectors connecting the six C_A atoms. The vector $\boldsymbol{u}^{(i)}$ was then defined as the average of the six normals obtained by the cross product of every pair of two neighboring C_A–C_A vectors. We calculated the orientational order tensor for each column and for the whole system,

$$Q_{\alpha\beta} = \left\langle \frac{1}{N}\sum_{i=1}^{N}\left(\frac{3}{2}u_{\alpha}^{(i)}u_{\beta}^{(i)} - \frac{1}{2}\delta_{\alpha\beta}\right)\right\rangle, \tag{5}$$

where $\boldsymbol{u}^{(i)}$ is a unit vector normal to the ith aromatic core and N is the number of molecules in a single column or in the whole system; correspondingly, the summation is performed

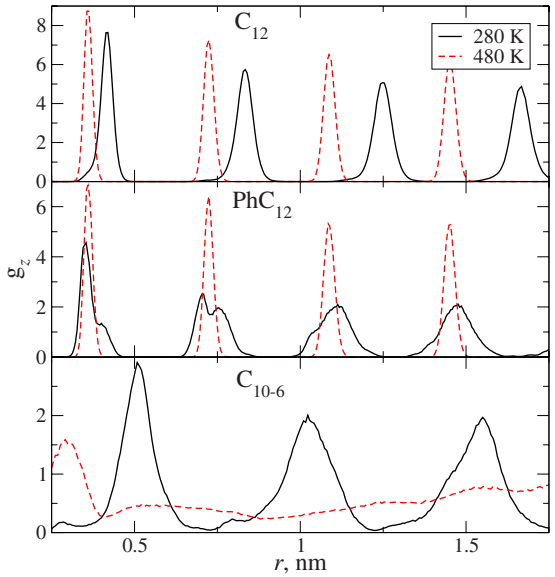

FIG. 7. (Color online) Distribution function characterizing the arrangement of the molecules in the plane parallel to the director $\boldsymbol{n}$, or direction of the columns, along the z axis.

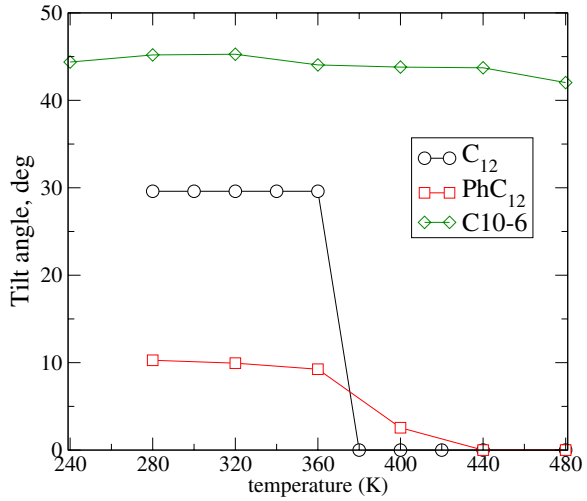

FIG. 8. (Color online) Average molecular tilt angle for all systems.

either over a single column or over the whole system. $\langle \cdots \rangle$ denotes the time average. Diagonalizing this tensor, we obtain the order parameter Q, which is the largest eigenvalue of $Q_{\alpha\beta}$, and the average orientation of the molecules, or director $\boldsymbol{n}$ (eigenvector corresponding to the eigenvalue Q). $Q=1$ implies perfect molecular alignment when all unit vectors are parallel to each other; $Q=0$ corresponds to the isotropic angular distribution of unit vectors.

In our case, the value of the nematic order parameter is always very close to 1 and practically does not change with temperature. The reason for this is the small system size constrained by the periodic boundary conditions. The less ordered system, namely, the one with C_{10-6} side chains, has at high temperature an order parameter of about 0.9 due to the fact that the domains still preserve a columnar structure. The average tilt angle, which is shown in Fig. 8, varies significantly from system to system as well as with temperature. The C_{12} system has the tilt angle of 30° in a herringbone mesophase and abruptly changes to zero at 380 K, at the same time as the symmetry of the lattice changes. The PhC_{12} system has a small tilt at low temperatures, which does not follow the herringbone pattern. This tilt gradually disappears once the temperature is increased, at the same time as the columns rearrange on a hexagonal lattice. The C_{10-6} system has a rather high tilt angle in the herringbone mesophase (45°). Here, the formation of domains with different tilt angles at higher temperatures preserves the average tilt angle in the system.

D. Intercolumnar diffusion

To show that the system is liquidlike at high temperatures, we calculated the mean-square displacement (MSD) of the molecular center of mass along the column direction (z axis),

$$\mathrm{MSD}(t) = \langle [z(t) - z(0)]^2 \rangle, \tag{6}$$

where the average is taken over all molecules.

The resulting profiles are shown in Fig. 9. The log-log profiles show that the MSD approaches a t^1 in the long-time limit, which is expected for a single-file diffusion,[32,33] when

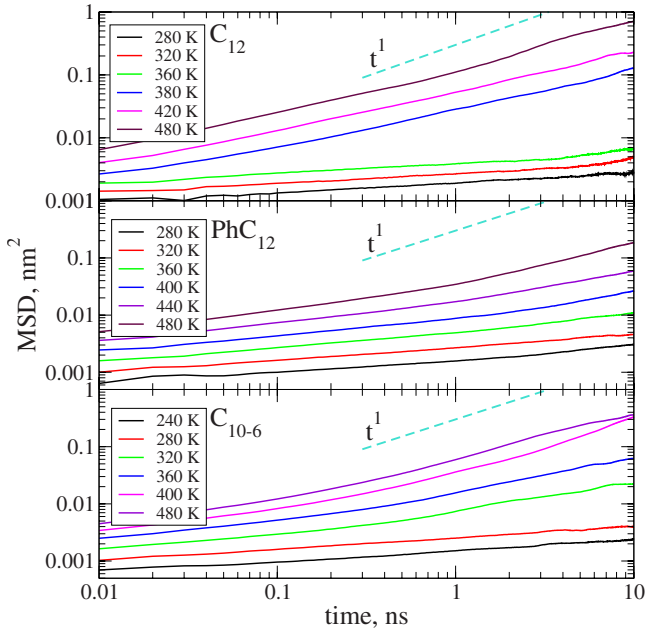

FIG. 9. (Color online) MSDs of the molecular center of mass along the column direction.

individual particles are unable to pass each other and the particle order remains the same over time, similar to what we observed before.[7]

For low temperatures, the log-log profiles show that the MSD has different asymptotics (smaller than $t^{1/2}$) than for $T=400$ K. The length of simulation runs does not allow us to conclude whether we have a frozen liquid crystalline state or a solid state but clearly points out that there is a transition from one phase to another. Interestingly, in the case of the PhC_{12} and C_{10-6} side chains the transition is rather smooth, contrary to the C_{12} side chains, where there are two distinct families of curves.

E. Azimuthal molecular ordering

Finally, one might ask the question whether the transition affects the azimuthal register of the neighbors in a column. To answer this question, the histograms of the azimuthal angle between two neighbors are shown in Fig. 10 for two representative temperatures, before and after the transition point. The first observation is that for both C_{12} and C_{10-6} the distributions undergo a major change: the maxima shifts from small angle at low temperature toward 30° in the liquid crystalline phase. In addition, C_{10-6} has much broader distributions compared to C_{12}. The distribution of the PhC_{12} system practically does not change since only the symmetry of the lattice changes but not the tilting of the molecules in columns. These changes in the distributions will no doubt affect the mobilities, as will be discussed in the second part of this contribution, due to the simple fact that the transfer integral is very sensitive to the mutual orientation of the neighbors.

IV. DISCUSSION AND CONCLUSIONS

We first compare our results to the existing experimental data. The system with the C_{12} side chains has a clear transi-

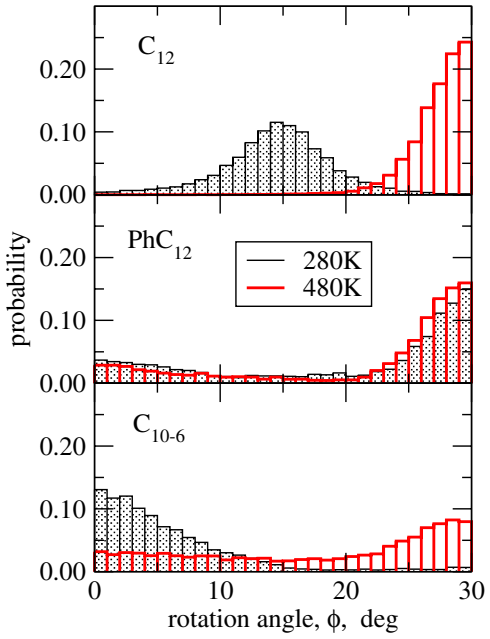

FIG. 10. (Color online) Distribution functions of the lateral twist angle between two neighboring molecules for two temperatures.

tion from a herringbone mesophase to a hexagonal mesophase. The transition temperature is at 380 K, which is, as well as the lattice constants of both mesophases, in a good agreement with experimental data.[12]

For PhC_{12} systems, experimental data predict that at low temperatures the herringbone phase is not formed. Our simulations confirm this observation: the herringbone phase becomes unstable already at room temperature and changes to the hexagonal arrangement of columns without significant molecular tilt in the columns. The reason for the absence of the herringbone phase is the steric repulsion of the twisted with respect to the core phenyl rings, which do not allow molecules to shift with respect to each other to allow tilting.[34]

At room temperature, the system with the C_{10-6} side chains is in the herringbone phase, which we also observe in simulations. The transition temperature to the columnar disordered phase is at 320 K, which compares to the experimental value of 290 K.[10] In simulations, we did find the experimentally observed transition to the isotropic phase at 370 K. This is, however, expected since our systems are rather small, 4×4 columns, and periodic boundary conditions stabilize the columnar mesophase. The lattice parameters for all systems are summarized in Table II.

We now turn the discussion on how the structural changes affect the mobility of charge carriers (holes in our case). Experimentally, phase transitions from phases with rectangular symmetry to those with hexagonal symmetry are accompanied by large reductions in mobility.[10,35] Charge transport characteristics will depend on the parameters governing charge transport, in particular, on the value of the transfer integral. The value of the transfer integral is greatest for adjacent molecules if they are displaced along the axis perpendicular to the molecular plane and are in the same orientation. This geometry, however, maximizes steric interaction between the side chains and does, therefore, not occur in practice. In phases with rectangular symmetry, adjacent hexabenzocoronene can minimize steric interaction by sliding over each other while maintaining the same orientation. In phase with hexagonal symmetry, instead, steric interactions are alleviated by rotating them about the column axis. This will lead to much smaller transfer integrals and, consequently, to lower mobilities. Systematic study of the influence of temperature-induced morphology change on mobility is the topic of the second part of this contribution.[21]

TABLE II. Lattice parameters for all studied systems. Lattice constants are given in nm. Simulation results are shown in bold. C_{12} and PhC_{12}: see Ref. 12. The simulated lattice parameters for the hexagonal mesophase are at 480 K, where the final configuration was the best equilibrated. C_{10-6}: see Refs. 10 and 36. Experimental value is at 333 K. Experimental data show a transition from a monoclinic cell (a=2.98 nm, b=2.50 nm, γ=60°) to the orthorhombic cell at 290 K and a transition to isotropic phase at 370 K. The simulation data were taken at 280 K. Starting from 320 K we observe a columnar disordered system.

C_{12}	Herringbone, 300 K		Hexagonal, 400 K	
a	**2.71**	3.05	**2.74**	2.86
b	**2.07**	2.38	$a=b$	
PhC_{12}	Orthorhombic, 300 K		Hexagonal, 400 K	
$a=b$	**2.86**	2.98	**3.21**	3.40
C_{10-6}	Orthorhombic			
a	**2.62**	4.32		
b	**2.14**	2.36		

ACKNOWLEDGMENTS

This work was partially supported by DFG via International Research Training Group between Germany and Korea and grant "Adaptive multiscale simulation for organic electronics." V.M. acknowledges Alexander von Humboldt foundation. J.K. acknowledges the EPSRC-GB. V.M., T.V., K.K., and D.A. acknowledge the Multiscale Materials Modeling Initiative of the Max Planck Society. Discussions with K. Müllen, H. W. Spiess, W. Pisula, R. Graf, and M. Mondeshki are gratefully acknowledged. C.J. and D.Y.Y. acknowledge the Chemistry and Molecular Engineering Program of Brain Korea 21 Project.

[1] F. Hoeben, P. Jonkheijm, E. Meijer, and A. Schenning, Chem. Rev. (Washington, D.C.) **105**, 1491 (2005).
[2] J. Wu, W. Pisula, and K. Müllen, Chem. Rev. (Washington, D.C.) **107**, 718 (2007).
[3] F. C. Grozema and L. D. A. Siebbeles, Int. Rev. Phys. Chem. **27**, 87 (2008).
[4] J. Kirkpatrick, V. Marcon, J. Nelson, K. Kremer, and D. Andrienko, Phys. Rev. Lett. **98**, 227402 (2007).
[5] D. Andrienko, J. Kirkpatrick, V. Marcon, J. Nelson, and K. Kremer, Phys. Status Solidi B **245**, 830 (2008).
[6] J. Kirkpatrick, V. Marcon, J. Nelson, and D. Andrienko, Phys. Status Solidi B **245**, 835 (2008).
[7] D. Andrienko, V. Marcon, and K. Kremer, J. Chem. Phys. **125**, 124902 (2006).
[8] V. Marcon, J. Kirkpatrick, W. Pisula, and D. Andrienko, Phys. Status Solidi B **245**, 820 (2008).
[9] A. M. van de Craats, J. M. Warman, A. Fechtenkotter, J. D. Brand, M. A. Harbison, and K. Müllen, Adv. Mater. **11**, 1469 (1999).
[10] W. Pisula, M. Kastler, D. Wasserfallen, M. Mondeshki, J. Piris, I. Schnell, and K. Müllen, Chem. Mater. **18**, 3634 (2006).
[11] A. M. van de Craats, L. Siebbeles, I. Bleyl, D. Haarer, Y. Berlin, A. A.

Zharikov, and J. Warman, J. Phys. Chem. B **102**, 9625 (1998).
[12] I. Fischbach, T. Pakula, P. Minkin, A. Fechtenkotter, K. Müllen, H. W. Spiess, and K. Saalwachter, J. Phys. Chem. B **106**, 6408 (2002).
[13] P. Herwig, C. W. Kayser, K. Müllen, and H. W. Spiess, Adv. Math. **8**, 510 (1996).
[14] S. P. Brown, I. Schnell, J. D. Brand, K. Müllen, and H. W. Spiess, J. Am. Chem. Soc. **121**, 6712 (1999).
[15] A. Fechtenkotter, K. Saalwachter, M. A. Harbison, K. Müllen, and H. W. Spiess, Angew. Chem. **38**, 3039 (1999).
[16] M. M. Elmahdy, X. Dou, M. Mondeshki, G. Floudas, H.-J. Butt, H. W. Spiess, and K. Müllen, J. Am. Chem. Soc. **130**, 5311 (2008).
[17] M. M. Elmahdy, G. Floudas, M. Mondeshki, H. W. Spiess, X. Dou, and K. Müllen, Phys. Rev. Lett. **100**, 107801 (2008).
[18] R. Berardi, L. Muccioli, and C. Zannoni, ChemPhysChem **5**, 104 (2004).
[19] P. L. Cristinziano and F. Lelj, J. Chem. Phys. **127**, 134506 (2007).
[20] G. Srinivas and M. L. Klein, Nanotechnology **18**, 205703 (2007).
[21] J. Kirkpatrick, V. Marcon, K. Kremer, J. Nelson, and D. Andrienko, J. Chem. Phys. **129**, 094506 (2008).
[22] A. Rybak, J. Pfleger, J. Jung, M. Pavlik, I. Glowacki, J. Ulanski, Z. Tomovic, K. Müllen, and Y. Geerts, Synth. Met. **156**, 302 (2006).
[23] M. Kastler, F. Laquai, K. Müllen, and G. Wegner, Appl. Phys. Lett. **89**, 252103 (2006).
[24] M. Carminati, L. Brambilla, G. Zerbi, K. Muellen, and J. Wu, J. Chem. Phys. **123**, 144706 (2005).
[25] S. Tsuzuki, T. Uchimaru, K. Matsumura, M. Mikami, and K. Tanabe, J. Chem. Phys. **110**, 2858 (1999).
[26] M. J. Frisch, G. W. Trucks, H. B. Schlegel *et al.*, GAUSSIAN 03, Revision C.02, Gaussian, Inc., Wallingford, CT, 2004.
[27] E. Lindahl, B. Hess, and D. van der Spoel, J. Mol. Model. **7**, 306 (2001).
[28] U. Essmann, L. Perera, M. Berkowitz, T. Darden, H. Lee, and L. Pedersen, J. Chem. Phys. **103**, 8577 (1995).
[29] B. Hess, H. Bekker, H. J. C. Berendsen, and J. G. E. M. Fraaije, J. Comput. Chem. **18**, 1463 (1997).
[30] K. J. Strandberg, *Bond Orientational Order in Condensed Matter Systems* (Springer, Berlin, 1992).
[31] W. Pisula, Z. Tomovic, M. Watson, K. Müllen, J. Kussmann, C. Ochsenfeld, T. Metzroth, and J. Gauss, J. Phys. Chem. B **111**, 7481 (2007).
[32] P. M. Richards, Phys. Rev. B **16**, 1393 (1977).
[33] M. Kollmann, Phys. Rev. Lett. **90**, 180602 (2003).
[34] C. Ochsenfeld, S. Brown, I. Schnell, J. Gauss, and H. Spiess, J. Am. Chem. Soc. **123**, 2597 (2001).
[35] M. Debije, J. Piris, M. de Haas, J. Warman, Z. Tomovic, C. Simpson, M. Watson, and K. Mullen, J. Am. Chem. Soc. **126**, 4641 (2004).
[36] W. Pisula, Ph.D. thesis, Max Planck Institute for Polymer Research, 2006.